

# A Peg-in-hole Assembly Strategy Using Uncalibrated Visual Servoing

Yeguo Liao, Weidong Chen, Hesheng Wang and Ruimin Wu

**Abstract**—This paper presents a novel peg-in-hole assembly strategy using uncalibrated visual servoing. A three phases assembly strategy is proposed to increase the workspace and avoid repeated desired features sampling when multiple holes are used. Depth-independent interaction matrix for vanishing point and point are derived and update rule for estimating unknown parameters is designed. A multiple phases alignment strategy is proposed to solve the coupled position and attitude issue. An uncalibrated kinematic-based controller is presented and asymptotic convergence is proved. Experiments are conducted to verify the performance.

**Index Terms**—pe-in-hole alignment, uncalibrated visual servoing

## I. INTRODUCTION

Peg-in-hole assembly is a common procedure in industrial and enabling robot to perform such task is of important significance for manufacturing automation. Since the robot operation has better consistency and traceability, thus product quality can be improved by replacing the manpower with robots. While peg-in-hole task in structured environment is well-addressed and satisfying result can be achieved using teaching by demonstration if tool is calibrated offline, difficulties arise for realizing peg-in-hole task in unstructured environment.

There are two issues for peg-in-hole task in unstructured environment, accurate tool calibration is infeasible and uncertainties appear in the pose of the hole. The former one occurs when the tool deforms slightly over time or quick change of different tools is required. The later one appears when one or both of the hole and robot are not fixed and the homogeneous transform matrix from robot base to hole can not be estimated offline. In metallurgy industry manufacturers, both of these issues emerge when performing task like inserting a contact rod (peg) into a metallurgical probe (hole). Contact rod deforms over time due to gravity and high temperature and rods with different parameters are used. To increase the workspace, the robot is installed on a rotation plate with inaccuracy axis encoder, which makes the transformation between robot base and the probe not fixed and can not be estimated offline.

Remote Center of Compliance (RCC)[1] or centering device are introduced to reduce the impact caused by the

This work is supported by the National Key R&D Program of China under grant 2017YFB1303600.

Yeguo Liao, Weidong Chen and Hesheng Wang are with Department of Automation, Shanghai Jiao Tong University and Key Laboratory of System Control and Information Processing, Ministry of Education of China. Ruimin Wu is with R&D Center, Baoshan Iron & Steel Co. Ltd. Corresponding Author: Weidong Chen(wdchen@sjtu.edu.cn).

issues mentioned above. However, these approaches only work in the situation where the alignment error between peg and hole is small. The tool may suffer from damage when the alignment error is beyond the tolerable range. A vision system provides non-contact information, which can be used as feedback to the control system and avoid violent impact. Visual servoing, also known as vision-based control, has been a hot topic in robotic manipulations research[2][3][4].

Lately, several works have been done to deal with the problem of peg-in-hole alignment. S. Liu *et al.*[5] proposed a robust insertion control method for precision peg-in-hole assembly. Their method relied on the estimated deformation of the passive compliance, which is not available in our case. J. Cao *et al.*[6] utilize the idea of depth-independent interaction matrix originally proposed in[7] and design an alignment method using points and lines. Their method avoids camera calibration and eliminates the effect of unknown depths in the controller. However, the working space is limited since a fixed camera is used. S. Huang *et al.*[8] proposed a visual compliance strategy for fast peg-and-hole alignment using two cameras. A multiple phases alignment strategy is designed to eliminate the effects caused by posture and position coupling.

In this paper, we utilize an eye-to-hand camera and extends the depth-independent matrix to the vanishing point. We proposed a three phases assembly strategy to increase the working space of the robot and avoid specifying desired features for each hole when multiple probes are used. A three steps alignment strategy is designed to solve the coupled position and attitude issue. A 3-d peg-in-hole alignment problem is transformed into an uncalibrated visual servoing problem with two points and a vanishing point extracted from the rod. The rest of the paper is organized as follows: The assembly strategy is detailed in section II. Section III addresses the modeling of the robot and the camera. The alignment strategy and the uncalibrated visual servoing controller are given in section IV. Experiments are conducted in section V to illustrate the performance of our method.

## II. PROBLEM STATEMENT AND ASSEMBLY STRATEGY

### A. Problem Definition

Considering the robot-magazine configuration shown in Fig 1, a six-axis robot equipped with a rod on its end-effector is installed on a rotation plate with inaccuracy axis encoder and the static probes are placed on the magazine. Our goal is to reduce the uncertainties caused by the rotation plate using



Fig. 1: Robot-magazine configuration

uncalibrated vision system and accomplish the peg-in-hole task.

### B. Notation

In this paper, matrices are shown in boldface letter, vectors in bold lower case letters and scalar quantities in italic letters.

Base frame, robot end-effector frame, predefined transition frame and camera frame are denoted by  $O_b$ ,  $O_e$ ,  $O_m$  and  $O_c$  respectively. The homogeneous transform matrix of the end-effector frame with respect to the base frame is denoted as  ${}^bT_e$ . When superscript and subscript are omitted,  $T$  denotes the homogeneous transform matrix of the end-effector frame with respect to the base frame.  $I_n$  denotes a  $n \times n$  identity matrix.

### C. Assembly Strategy

The robot is installed on a rotation plate to increase the workspace. The radius of the rotation plate is about 2000 mm and the axis encoder is inaccurate, which reduces the repeatability of the robot and makes the teaching method invalid. We propose a three phases strategy (see Fig 2) which allows the robot to work in a large range of workspace.

1) *phase 1*: The robot and the rotation plate move together to reach the magazine when the end-effector is far away from the magazine. At the end of this phase, the tip of the rod is positioned under a camera mounted on the magazine as shown in Fig 3.

2) *phase 2*: A camera is used to monitor the rod and provide visual feedback to control the robot's motion. Assuming that the camera and the rod are uncalibrated, we use an uncalibrated visual servoing algorithm to guide the rod to a predefined transition location  $O_m$ . The rotation plate is fixed in this phase.

3) *phase 3*: Considering that the homogeneous transform matrices from the frame  $O_m$  to each probe are known and fixed. In this phase, the rod is moved to the front of the probe and then inserted into the probe using PTP motion while the rotation plate remains fixed.

The remains of this paper focus on the uncalibrated visual servoing algorithm used in phase 2.

## III. MODELING

### A. Robot modeling

The robot end-effector pose is denoted by a 6-dimensional vector  $r(t) = [v(t), \omega(t)]^T$ , where  $v(t)$  and  $\omega(t)$  denote the linear velocities and angular velocities of the robot end-effector respectively.

The homogenous transform matrix of the end-effect frame with respect to the base frame can be rewrite as

$${}^bT_e(r(t)) = \begin{bmatrix} R(r(t)) & \xi(r(t)) \\ 0 & 1 \end{bmatrix} \quad (1)$$

where  $R(r(t))$  and  $\xi(r(t))$  are the rotation matrix and the translation vector respectively.

### B. Camera model

A pin-hole camera model is used in this paper. Denote the camera intrinsic matrix by  $\Omega$  and extrinsic matrix by  ${}^bT_c$ . Denote a fixed 3-D point in end-effector frame by  ${}^e x$  and its projection on the image plane by  $y(t)$ , the relationship between  ${}^e x$  and  $y(t)$  is given by

$$\begin{bmatrix} y(t) \\ 1 \end{bmatrix} = \frac{\Omega {}^c T_b T(r(t))}{{}^c z(t)} \begin{bmatrix} {}^e x \\ 1 \end{bmatrix} = \frac{M T(r(t))}{{}^c z(t)} \begin{bmatrix} {}^e x \\ 1 \end{bmatrix} \quad (2)$$

where  $M$  is the unknown projection matrix, which is the product of camera intrinsic and extrinsic matrix. Denote  $M_{12}$  and  $m_3^T$  as the first two rows and third row of  $M$  respectively, the projection relationship can be rewritten as :

$${}^c z(t) y(t) = M_{12} T(r(t)) \begin{bmatrix} {}^e x \\ 1 \end{bmatrix} = p(r(t)) \quad (3)$$

$${}^c z(t) = m_3^T T(r(t)) \begin{bmatrix} {}^e x \\ 1 \end{bmatrix} \quad (4)$$

The time derivative of  $y(t)$  and  ${}^c z(t)$  can be written as

$${}^c \dot{z}(t) = m_3^T \begin{bmatrix} I_3 & -sk(R(t)) {}^e x \\ 0_{1 \times 3} & 0_{1 \times 3} \end{bmatrix} \dot{r}(t) = a^T(t) \dot{r}(t) \quad (5)$$

$${}^c z(t) \dot{y}(t) = \frac{\partial M_{12} T(r(t))}{\partial r} \begin{bmatrix} {}^e x \\ 1 \end{bmatrix} - \frac{\partial {}^c z(t)}{\partial r} y(t) = A(t) \dot{r}(t) \quad (6)$$

Note that  $A(t)/{}^c z(t)$  is the interaction matrix and  $A(t)$  is defined as depth-independent interaction matrix[7]. Given a homogeneous vector  $\rho$ , the product of  $A(t)$  and  $\rho$  can be rewritten as a linear combination of unknown parameters  $\theta$  and a constant vector  $\sigma$ [9].

$$A(t) \rho = Q(\rho, y(t)) \theta + \sigma \quad (7)$$

where  $Q(\rho, y(t))$  is a regression matrix and does not depend on unknown parameters.



(a) Phase 1



(b) Phase 2



(c) Phase 3

Fig. 2: Assembly strategy

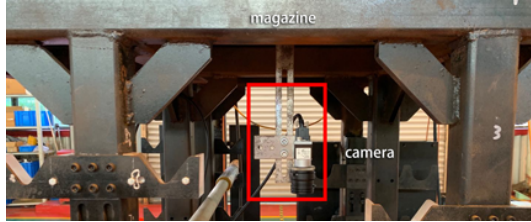


Fig. 3: Camera configuration

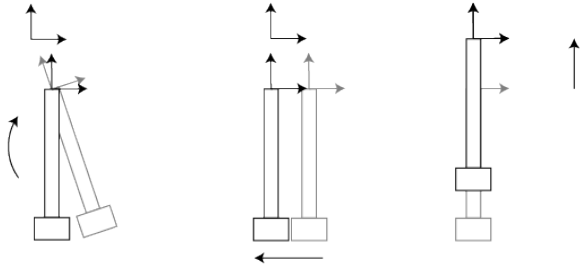


Fig. 4: Alignment strategy

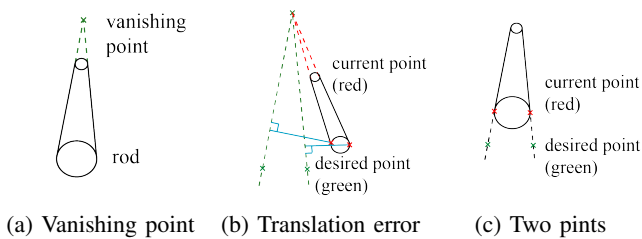


Fig. 5: Image features

#### IV. UNCALIBRATED VISUAL SERVOING

Vision feedback is used to guide the rod to realize its alignment with the predefined frame  $O_m$ . Conventional visual servoing method can not achieve a fast and accurate alignment since the adjustment of the position and attitude of the rod are coupled[8].

##### A. Alignment Strategy

In this paper, a three phases visual servoing alignment strategy (See Fig 4) is presented to solve the difficulties mentioned above.

*1) Attitude alignment:* We first align the longitudinal axis of the rod to its desired orientation using vanishing point (See Fig 5a). At the end of this step, the longitudinal axis of the rod is parallel to its desired orientation while the rotation along the longitudinal axis is ignored.

Any line in 3-D space can be defined as a combination of a point and a direction vector, i.e.,  $p_0 + tu$ . The projections of any line parallel to  $u$  on the image plane meet at a vanishing point, which is the projection of  $[u^T, 0]^T$ . Denote the intersection of two lines of rod edge as  $y_v(t)$ , which is the projection of  $[r_3^T(t), 0]^T$ , where  $r_3(t)$  is the third column of  $R(t)$ . Define the image error for vanishing point as

$$\Delta y_v(t) = y_v(t) - y_{vdes} \quad (8)$$

where  $y_{vdes}$  is the desired vanishing point. When the image error of vanishing point is less than  $threshold_v$ , the longitudinal axis of the rod is considered to be parallel to its desired orientation and switch to collinearity alignment phase.

*2) Collinearity alignment:* The rod is moved to make its longitudinal axis collinear with its desired longitudinal axis. Denote two intersection points formed by lines mentioned above and the end face of the rod and their desired coordinate as  $y_{pi}(t)$  and  $y_{pd_{si}}$  respectively, where  $i = 1, 2$ . When the longitudinal axis of the rod is collinear with its desired position,  $y_{pi}(t)$  fall on the line formed by connecting desired vanishing point  $y_{vdes}$  and  $y_{pd_{si}}$ . Defined translation error  $\Delta y_{di}(t)$  as the vector start from  $y_{pi}$  and vertical to the line formed by connecting desired vanishing  $y_{vdes}$  and  $y_{pd_{si}}$ . (The blue lines in Fig 5b). We switch to next the phase when the translation error is less than  $threshold_{transl}$ .

*3) Longitudinal alignment:* At the end of collinearity alignment phase, there is a longitudinal error between the current position of the rod and its desired position(See Fig 5c). We defined a longitudinal error as

$$\Delta y_{pi}(t) = y_{pi}(t) - y_{pd_{si}}, i = 1, 2 \quad (9)$$

When longitudinal error is less than one pixel, the rod is considered to alignment with the frame  $O_m$ .

### B. Controller

Denote the features and their image errors by  $y_i(t)$  and  $\Delta y_i(t)$  respectively.

$$y_i(t) = \begin{cases} y_v(t) & \text{for attitude alignment} \\ y_{p_i}(t) & \text{for collinearity and} \\ & \text{longitudinal alignment} \end{cases} \quad (10)$$

$$\Delta y_i(t) = \begin{cases} \Delta y_v(t) & \text{for attitude alignment} \\ \Delta y_{d_i}(t) & \text{for collinearity alignment} \\ \Delta y_{p_i}(t) & \text{for longitudinal alignment} \end{cases} \quad (11)$$

Inspired by [6], a kinematic-base controller is designed as follows

$$\dot{r} = -\sum_{i=1}^n (\hat{A}_i^T(t) + \frac{1}{2}\hat{a}_i(t)\Delta y_i^T(t))K_{1i}\Delta y_i(t) \quad (12)$$

where  $K_{1i}$  is a constant positive definite gain matrix for each feature and  $n = 1, 2, 2$  for attitude alignment, collinearity alignment and longitudinal alignment respectively.

According to equation (7), the designed controller can be rewritten as

$$\begin{aligned} & -(\hat{A}_i^T(t) + \frac{1}{2}\hat{a}_i(t)\Delta y_i^T(t))K_{1i}\Delta y_i(t) \\ & = -(A_i^T(t) + \frac{1}{2}a_i(t)\Delta y_i^T(t))K_{1i}\Delta y_i(t) + \\ & Y_i(r(t), y_i(t))\Delta\theta_i(t) \end{aligned} \quad (13)$$

where  $Y_i(r(t), y_i(t))$  is a regression matrix independent of unknown parameters and  $\Delta\theta_i(t) = \hat{\theta}_i(t) - \theta_i$  is the error of parameters estimation for each feature.

### C. Parameter Estimation

The unknown parameters can be estimated from an adequate number of images acquired when the robot is in motion and can only be estimated up to a scale [9]. To avoid trivial solution, one can fix one element of each parameters set.

According to (7), We defined and linearized the parameters estimation error function as

$$e_i(t) = {}^c\hat{z}(t)y_i(t) - \hat{p}(r(t)) = W_i(r(t), y_i(t))\Delta\theta_i(t) \quad (14)$$

where  $W_i(r(t), y_i(t))$  is a regression matrix independent of unknown parameters.

An adaptive parameter update rule[9] is designed as follows to minimize the estimation error function,

$$\begin{aligned} \dot{\hat{\theta}}_i(t) & = -K_{2i}^{-1}\{Y_i^T(r(t), y_i(t))\dot{q}(t) + \\ & \sum_{j=1}^k W_i^T(r(t_j), y_i(t_j))K_{3i}e_i(t_j)\} \end{aligned} \quad (15)$$

where  $K_{2i}$  and  $K_{3i}$  are constant positive definite gain matrices for each feature.

### D. Stability Analysis

The stability of the designed controller is proved by Lyapunov theory. Given that all the features stay in the field of view during the whole visual servoing task. A positive definite candidate function similar to the one in [6] is defined as

$$V(t) = \frac{1}{2}\sum_{i=1}^n({}^cz_i(t)\Delta y_i^T(t)K_{1i}\Delta y_i(t) + \Delta\theta_i^T(t)K_{2i}\Delta\theta_i(t)) \quad (16)$$

Multiplying  $\dot{r}^T(t)$  on both sides of equation (12), we obtain

$$\begin{aligned} \dot{r}^T(t)\dot{r}(t) & = -\dot{r}^T(t)\sum_{i=1}^n(A_i^T(t) + \frac{1}{2}a_i(t)\Delta y_i^T(t))K_{1i}\Delta y_i(t) \\ & + \sum_{i=1}^nY_i(r(t), y_i(t))\Delta\theta_i(t) \end{aligned} \quad (17)$$

Multiplying  $\Delta\theta^T(t)$  on both sides of equation (15), we obtain

$$\begin{aligned} \Delta\theta_i^T(t)K_{2i}\Delta\dot{\theta}_i(t) & = -\Delta\theta_i^T(t)Y_i^T(r(t), y_i(t))\dot{r}(t) \\ & - \sum_{j=1}^k e_i^T(t_j)K_{3i}e_i(t_j) \end{aligned} \quad (18)$$

Differentiating the Lyapunov candidate function (16) and combine (17) and (18), we obtain

$$\begin{aligned} \dot{V}(t) & = \frac{1}{2}\sum_{i=1}^4{}^cz_i(t)\Delta y_i^T(t)K_{1i}\Delta y_i(t) \\ & + \sum_{i=1}^4{}^cz_i(t)\Delta y_i^T(t)K_{1i}\Delta\dot{y}_i(t) + \sum_{i=1}^4\Delta\theta_i^T(t)K_{2i}\Delta\dot{\theta}_i(t) \\ & = -\dot{r}^T(t)\dot{r}(t) - \sum_{i=1}^4\sum_{j=1}^k e_i^T(t_j)K_{3i}e_i(t_j) \end{aligned} \quad (19)$$

$\Delta y(t)$ ,  $\Delta\theta(t)$ ,  $\Delta e_i(t_j)$  and  $\dot{r}(t)$  are all bounded since equation (19) is negative.

Differentiating equation (19) results in

$$\ddot{V}(t) = -2\ddot{r}^T(t)\ddot{r}(t) - 2\sum_{i=1}^4\sum_{j=1}^k e_i^T(t_j)K_{3i}e_i(t_j) \quad (20)$$

which is bounded. From Barbalats lemma, we have

$$\begin{aligned} \lim_{t \rightarrow \infty} \dot{r}(t) & = 0 \\ \lim_{t \rightarrow \infty} e_i(t) & = 0 \\ \lim_{t \rightarrow \infty} \dot{\hat{\theta}}_i(t) & = 0 \end{aligned} \quad (21)$$

The asymptotic convergence of the end-effector velocity, projection estimation error and parameters estimation error

can be proved based on the above discussion. It can be proved that when the number of the joint variable is equal to 6 or is greater than two times the number of the image features, the image errors converge to zero [7][10].

## V. EXPERIMENT



Fig. 6: Initial robot configuration

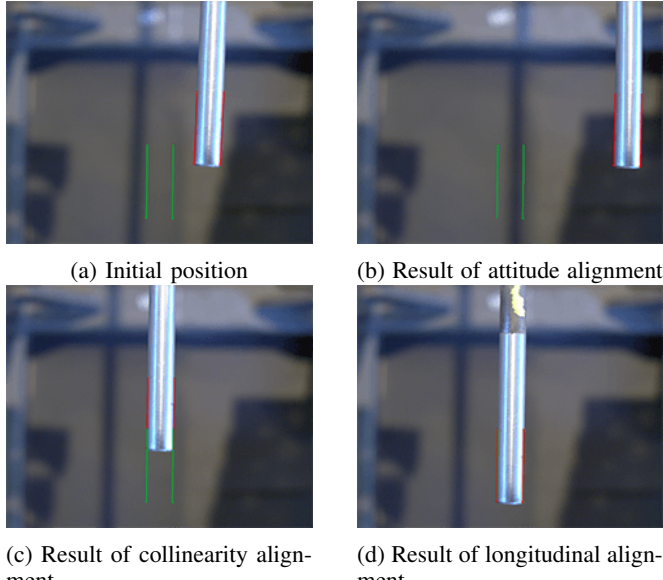


Fig. 7: Camera view

Experiments are carried out to illustrate the performance of our method. A KUKA KR210 robot and a Basler acA2500-60u camera equipped with a 15 mm lens are used. The robot is installed on a rotation plate with inaccuracy axis encoder. A rod that is 1500 mm long and 16 mm in diameter is mounted at the end-effector. The probes are fixed on the magazine and the diameter of their opening is 18 mm. The camera is installed on the underside of the top of the magazine. The angle between the optical axis of the camera and the ground is about 20°. The initial value of the projection matrix can be obtained from coarse camera calibration.

The initial robot configuration is shown in Fig 6. The robot and the rotation plate move together to reach the magazine

when the end-effector is far away from the magazine (Assembly strategy phase 1). We simply use PTP motion in this step. Due to the inaccuracy axis encoder of the rotation plate, the resulting repeat positioning error of the tooltip is in the range of (-50 mm, 50 mm). The proposed alignment strategy is then used to eliminate repeat the positioning error (Assembly strategy phase 2).

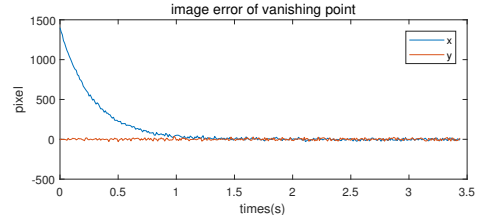


Fig. 8: Image error of vanishing point

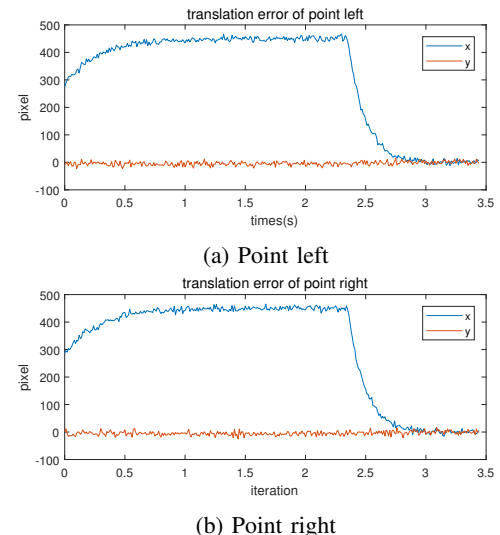


Fig. 9: Translation error

### A. Attitude alignment

In the attitude alignment step, we extract two lines from the rod edge (See Fig 7a). Moving line tracker from ViSP[11] is utilized to reduce the time spent on image processing. The lines in red are the current projection of the rod edge while lines in green are the desired locations. The vanishing point can be obtained from the interception of the lines and is usually outside the field of view of the camera. The control parameters are fine-tuned and the following values are used:  $K_{11} = 5e^{-8}I_2$ ,  $K_{21} = 1e^3I_9$ ,  $K_{31} = 1e^{-4}I_2$ ,  $threshold_v = 1$ . The result of attitude alignment is shown in Fig 7b, where the currently observed vanishing point coincided with the desired one. The image error of vanishing point is shown in Fig 8. We can observe that the image error of vanishing point is less than  $threshold_v$  after 4.3 s.

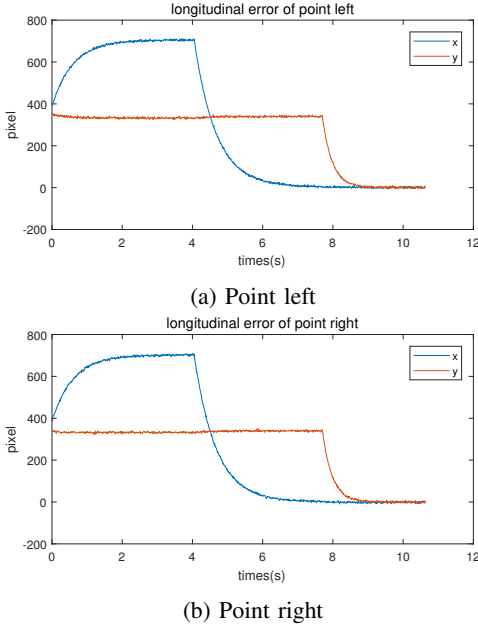


Fig. 10: Longitudinal error

### B. Collinearity alignment

Two points are extracted from the interceptions of the end face and the lines used in the last step. The control parameters are fine-tuned and the following values are used:  $K_{12} = 2e^{-7}I_2$ ,  $K_{22} = 1e^3I_9$ ,  $K_{32} = 1e^{-4}I_2$ ,  $\text{threshold}_{\text{transl}} = 0.1$ . The result of collinearity alignment is shown in Fig 7c, where the currently observed points fall on the lines formed by connecting the desired vanishing point and the desired points. The translation error is shown in Fig 9. It is worth noting that the translation error keeps increasing during attitude alignment but start to decrease when switching to collinearity alignment phase at 4.3 s.

### C. Longitudinal alignment

The points used in the last step are re-used to measure the longitudinal error. The control parameters are fine-tuned and the following values are used:  $K_{13} = 2e^{-7}I_2$ ,  $K_{23} = 1e^3I_9$ ,  $K_{33} = 1e^{-4}I_2$ . The result of longitudinal alignment is shown in Fig 7d, where the currently observed points in red coincided with the desired points in green. The longitudinal error is shown in Fig 10. We can observe that the controller switches to the longitudinal alignment phase and the longitudinal error is less than one pixel at 11 s.

At the end of the longitudinal alignment, the rod is alignment with the predefined transition frame  $O_m$ . Since the transformation from frame  $O_m$  to each probe is known, the rod is then moved to the front of the probe and then inserted into its opening using PTP motion while the rotation plate remains fixed (Assembly strategy phase 3, see Fig 2c).

## VI. CONCLUSIONS

In this paper, we proposed a assembly strategy for peg-in-hole alignment task. A vision system with an eye-to-hand mono camera is utilized to observing features on the tool. By using a predefined transition location, we increase the workspace of the robot and avoid specifying desired features for each hole when multiple probes are used. By taking the camera intrinsic and extrinsic parameters and tool parameters as unknown parameters together, we implement visual servoing based on the depth-independent interaction matrix framework. we designed a three phases alignment strategy using one vanishing point and two contour points to solve the coupled position and attitude issue. Depth-independent interaction matrix for features are deduced and A kinematic-based controller is designed. To estimate unknown parameters online and guarantee the stability of controller, parameter update rule is given. Asymptotic convergence of the image errors to zero is rigorously proved by Lyapunov theory. The performance of our method is illustrated by experiments conducted on a KUKA KR210 robot. The result has shown the tool pose converged to the desired pose and inserted into the probes successfully.

## REFERENCES

- [1] D. E. Whitney. Quasi-Static Assembly of Compliantly Supported Rigid Parts. *Journal of Dynamic Systems, Measurement, and Control*, 104(1):65–77, 03 1982.
- [2] S. Hutchinson, G. D. Hager, and P. I. Corke. A tutorial on visual servo control. *IEEE Transactions on Robotics and Automation*, 12(5):651–670, Oct 1996.
- [3] F. Chaumette and S. Hutchinson. Visual servo control. i. basic approaches. *IEEE Robotics Automation Magazine*, 13(4):82–90, Dec 2006.
- [4] F. Chaumette and S. Hutchinson. Visual servo control. ii. advanced approaches [tutorial]. *IEEE Robotics Automation Magazine*, 14(1):109–118, March 2007.
- [5] S. Liu, D. Xing, Y. Li, J. Zhang, and D. Xu. Robust insertion control for precision assembly with passive compliance combining vision and force information. *IEEE/ASME Transactions on Mechatronics*, 24(5):1974–1985, Oct 2019.
- [6] J. Cao, H. Wang, W. Chen, J. Wang, and R. Wu. Uncalibrated peg-hole alignment using visual servoing. In *2017 IEEE International Conference on Real-time Computing and Robotics (RCAR)*, pages 549–554, July 2017.
- [7] Y. Liu, H. Wang, C. Wang, and K. Lam. Uncalibrated visual servoing of robots using a depth-independent interaction matrix. *IEEE Transactions on Robotics*, 22(4):804–817, Aug 2006.
- [8] S. Huang, K. Murakami, Y. Yamakawa, T. Senoo, and M. Ishikawa. Fast peg-and-hole alignment using visual compliance. In *2013 IEEE/RSJ International Conference on Intelligent Robots and Systems*, pages 286–292, Nov 2013.
- [9] H. Wang, Y. Liu, and D. Zhou. Adaptive visual servoing using point and line features with an uncalibrated eye-in-hand camera. *IEEE Transactions on Robotics*, 24(4):843–857, Aug 2008.
- [10] H. Wang, B. Yang, J. Wang, X. Liang, W. Chen, and Y. Liu. Adaptive visual servoing of contour features. *IEEE/ASME Transactions on Mechatronics*, 23(2):811–822, April 2018.
- [11] E. Marchand, F. Spindler, and F. Chaumette. ViSP for visual servoing: a generic software platform with a wide class of robot control skills. *IEEE Robotics Automation Magazine*, 12(4):40–52, Dec 2005.